Comparative study on various sponges as substrates for reduced graphene oxide-based supercapacitor

Dongcheol Choi and Kyuwon Kim♣

Department of Chemistry, Incheon National University, Incheon 22012, Korea
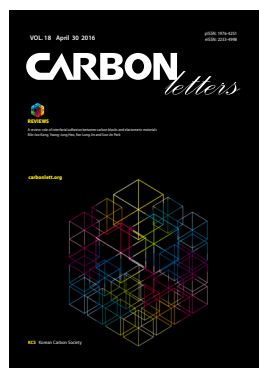
To solve environmental problems and address the exhaustion of fossil fuel resources, the development of environmentally friendly and alternative energy storage devices has attracted much interest. Supercapacitors are attractive devices for such a purpose because of their high power density, long cycle life, low maintenance, wide range of operating temperatures, and fast charging time compared to conventional capacitors and batteries [1-5]. Supercapacitors can be divided into two general classes characterized by their unique mechanism for storing charge. The first class includes electrochemical double layer capacitors (EDLCs), which store a charge electrostatically or non-faradically, when the charge is distributed over surfaces through physical processes. EDLCs generally operate with stable capacitive performance for many charge-discharge cycles because there are no chemical or compositional changes. The second class is called pseudocapacitors. These store a charge faradically through redox reactions and electrosorption at the surface of a suitable electrode. Pseudocapacitors can achieve greater energy densities than EDLCs [5-8]. Graphene materials, which consist of a few atomic layers of only graphite, have attracted great interest as novel electrode materials for energy storage devices because of their superior properties and advantages, such as high electrical and thermal conductivity, great mechanical strength, large specific surface area, and low manufacturing cost [9-13]. In this work, reduced graphene oxide (RGO), obtained through the chemical reduction of graphene oxide (GO), was used as a capacitive material [14-16]. Here, sponges similar to the ones used in ordinary life have been employed as supporting substrates for the fabricated supercapacitor electrodes. Sponges have suitable properties for improving capacitive performance, such as good wettability, highly porous structure, and substantial internal surface area. In demonstrations, they have provided smooth accessibility of ions to electrolytes. Among the various sponges easily available on the market, three types have been employed: polyvinyl alcohol (PVA), melamine, and polyurethane (PU) sponges. The capacitive performances of these types of sponge were compared. A facile dip and dry method was demonstrated, using an RGO solution to coat each sponge, to fabricate an RGO-coated sponge (RGO-sponge) electrode without additional binder and or conductive materials [17-19].

All chemical reagents including graphite powder (<20 μm) were purchased from Sigma Aldrich (USA). PVA sponge and Melamine sponge were purchased from CJ Olive Young, and PU sponge was purchased from Spongemart in the Republic of Korea. Elemental analysis was performed using a Flash 2000 (Thermo Scientific, UK). Atomic force microscopy (AFM) was performed using a Nano-R (Pacific Nanotechnology, USA). Attenuated total reflection Fourier transform infrared (ATR-FTIR) measurements were performed by a Vertex 80V (Bruker Optics, Germany). Raman spectroscopy was performed by an Alpha 300 (WITec , Germany). The Brunauer-Emmett-Teller specific surface area (BET-SSA) was measured using a Tristar, ASAP2020 (Micromeritics, USA). Electrochemical measurements, including cyclic voltammetry (CV) and galvanostatic charge-discharge tests, were conducted with an Ivium Compactstat potentiostat (B0714).

A GO suspension was synthesized from graphite powder using a modified Hummers method. The RGO was obtained by simple chemical reduction from GO. An RGO solution was obtained using ammonium hydroxide, with hydrazine hydrate as a reducing agent,
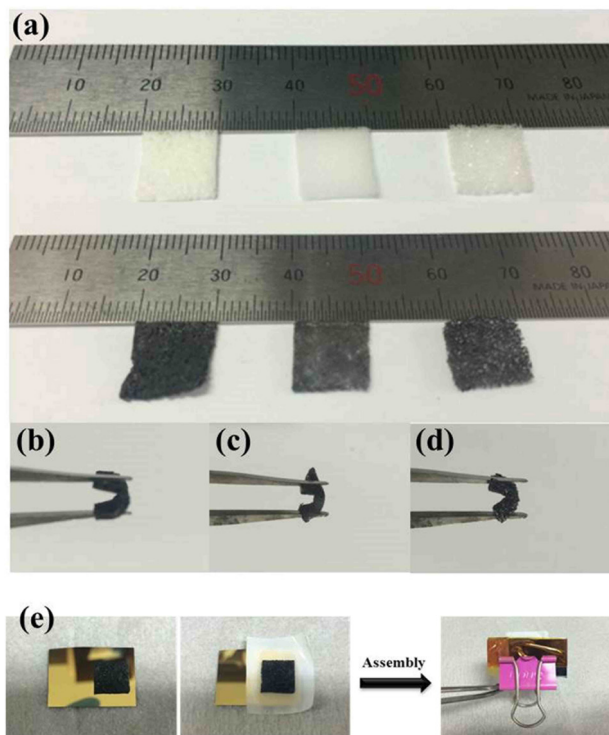
Fig. 1. (a) Photograph of unmodified (left to right) PVA, melamine, and PU sponge (upper); and RGO-coated (left to right) PVA, melamine, and PU sponge (bottom). (b) Photograph of a flexible RGO-coated (b) PVA, (c) melamine, and (d) PU sponge. (e) Assembly process for a two-electrode cell.

PVA, polyvinyl alcohol; PU, polyurethane; RGO, reduced graphene oxide.

Fig. 2. (a) Attenuated total reflection Fourier transform infrared spectra of graphene oxide (GO) and reduced graphene oxide (RGO); atomic force microscope images and height profile of a single layer of (b) GO and (c) RGO.

under N_2 gas. First, ammonium hydroxide was added to adjust the pH to 10.5 in the GO solution (0.5 mg/mL). Then, 55 µL of hydrazine hydrate was added and stirred magnetically for 5 min. The solution was heated at 95°C for 2 h. After reduction, this aqueous solution was centrifuged to remove precipitates of the aggregated RGO sheets.

The RGO-sponge electrode was fabricated using a very facile method in which the sponge was dipped in the RGO solution and then dried. Three types of sponges (PVA, melamine, and PU) were cleaned with distilled water, acetone, and ethanol several times, dried completely in a vacuum oven at 100°C for 3 h, and cut into small pieces (thickness ~1 mm and area 1.0 × 1.0 cm). The sponge pieces were dipped into 0.2 mg/mL of the RGO solution and then dried in a vacuum oven at 100°C for 10 min. This was repeated five times to increase the amount of RGO loaded. Then, the sponges were cleaned thoroughly with distilled water to remove impurities produced in the process of synthesizing the RGO solution. After this, the RGO-sponges were dried in a vacuum oven at 100°C for 3 h to remove the water completely. Fig. 1a shows the three types of fabricated RGO-sponges. In this paper, three types of fabricated RGO-sponges were mentioned, including the RGO-PVA sponge, RGO-melamine sponge, and RGO-PU sponge, respectively. The upper images are unmodified sponges and the bottom images are RGO-sponges (from left, PVA, melamine, and PU sponges). The three types of RGO-sponges in Fig. 1b-d show the mechanical flexibility of each
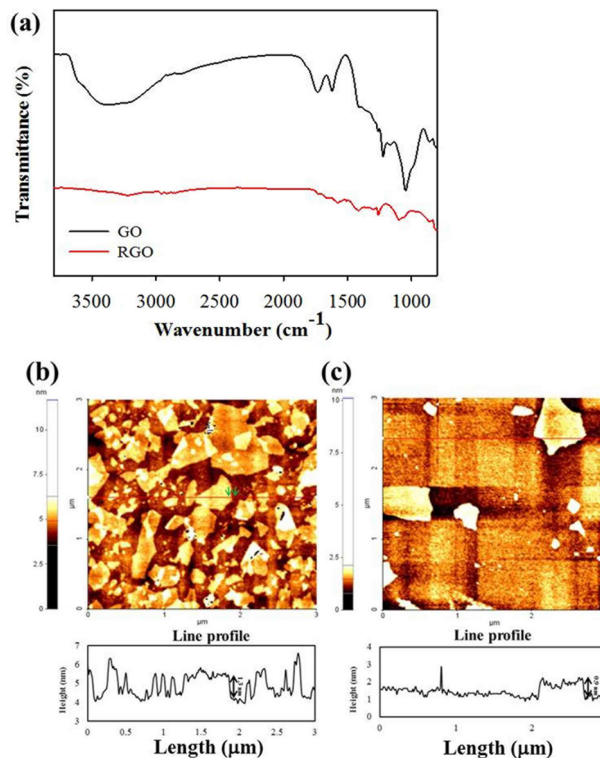
RGO-sponge. The loaded amount of RGO on each RGO-sponge was ~0.05 mg after soaking in the RGO solution and drying, five times. The mass of the loaded RGO was determined by weighing the sponge before and after RGO coating using an electronic microbalance.

The electrochemical measurements were conducted using a two-electrode system. Two pieces of RGO-sponge were used as both electrodes, and they were separated by filter paper (Celgard 3501, USA) soaked with 1 M H_2SO_4 as an electrolyte. Two gold-coated glasses were used as the current collectors. All of the components were assembled into a layered structure and sandwiched between two gold-coated glasses [20]. Fig. 1e shows the process of assembling the two-electrode cell. The electrochemical performance of the supercapacitor cells was evaluated using CV and a galvanostatic charge-discharge test. CV was performed in the potential range 0–1 V at different scan rates from 10 to 1000 mV/s. The galvanostatic charge-discharge curves were obtained in the potential range 0–1 V at different current densities (from 1 to 30 A/g). All electrochemical capacitive performance tests were performed in 1 M H_2SO_4 as an electrolyte for electrochemical reactions in the cell.

The chemical compositions of GO and RGO were characterized by elemental analysis. This result shows an increase in the carbon to oxygen atomic ratio of RGO (4.78) compared with 1.19 for GO. This means a sufficient reduction in the oxygen-functional groups of GO by hydrazine. The attenuated total reflectance (ATR-FTIR) was also measured to characterize
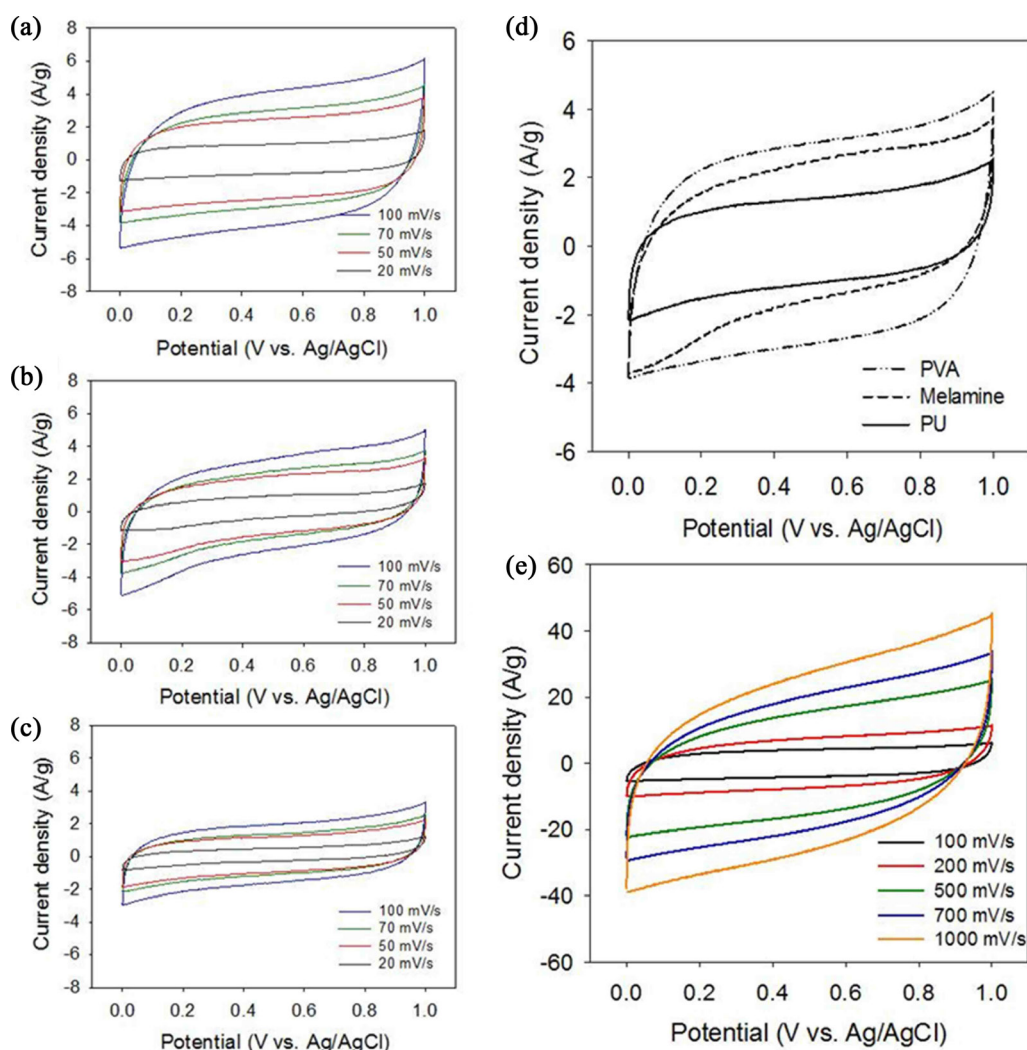
Fig. 3. Cyclic voltammograms of RGO coated (a) PVA, (b) melamine, and (c) PU sponge at different scan rates (20–100 mV/s) in the range 0–1 V of potential. Cyclic voltammograms of (d) RGO coated PVA, melamine, and PU sponge at the scan rate of 70 mV/s, and (e) RGO coated PVA sponge at different scan rates (100–1000 mV/s) in the range 0–1 V of potential.
RGO, reduced graphene oxide; PVA, polyvinyl alcohol; PU, polyurethane.

the synthesis of RGO. In Fig. 2a, GO shows obvious peaks at 3300, 1730, and 1050 cm^{-1}, which correspond to the O-H bond, O-C=O groups, and C-O-C groups, respectively. After the reduction of GO, most peaks involved in the oxygen-containing functional groups were decreased considerably, which indicates successful reduction of GO. Fig. 2b and c show AFM images of GO and RGO, respectively, on an (3-Aminopropyl)triethoxysilane (APTES)-modified silicon surface. The measured thickness from the height profile was about 1.3 nm, as reported previously, indicating a single layered GO [21]. After the reduction of GO by hydrazine, the measured thickness of the RGO was about 0.9 nm. This value is smaller than that of GO because of the elimination of oxygen-functional groups, and it is comparable to the previously reported thickness of an RGO sheet [22,23]. In the result from Raman spectroscopy of GO and RGO, the I_D/I_G ratio of RGO (1.164) increased, compared to that of GO (0.938). This indicates a structural change caused by the structural defects of

GO, and a decrease in the size of the in-plane sp^2 domains by a reduction of the oxygen-functional groups of GO [15].

CV and galvanostatic charge-discharge tests were conducted in 1 M H_2SO_4 as electrolyte with a two-electrode system to measure the capacitive performance. CV was conducted in the potential range 0–1 V at different scan rates. Fig. 3a-c show the CV curves of the RGO-PVA, melamine, and PU sponges at different scan rates (from 20 to 100 mV/s). All of the CV curves of the three types of RGO-sponge show a quasi-rectangular shape, which characterizes the electrochemical double layer capacitive behavior of the loaded RGO [1,24,25]. The sponges used in this test are intrinsic insulators for which no current conduction has been observed. Fig. 3d illustrates the CV curve of the RGO-PVA sponge to show the largest area. This indicates a larger specific capacitance of the RGO-PVA sponge than of the RGO-melamine and RGO-PU sponges. This difference is affected by the specific surface area or surface properties of the electrode.

Table 1. BET-SSA results: average pore width of PVA, melamine, and PU sponge

Sample	BET-SSA (m²/g)	Average pore width (Å)
PVA	0.3197	133.0763
Melamine	1.4420	116.7731
PU	0.4400	170.6670

BET-SSA, Brunauer-Emmett-Teller specific surface area; PVA, polyvinyl alcohol; PU, polyurethane.

The BET-SSA of the PVA, melamine, and PU sponges was estimated to be 0.3197, 1.4420, and 0.4400 m²/g, respectively; and the average pore width of the PVA, melamine, and PU sponges were estimated to be 133.0763, 116.7731, and 170.6670 Å, respectively (Table 1). The BET surface area of the melamine sponge is greater than that of the PU sponge. Although the BET surface area of the PVA sponge is the smallest among them, the CV curve of the RGO-PVA sponge shows the largest area. This result is mainly because the PVA sponge is extremely hydrophilic due to abundant hydroxyl groups. The hydroxyl groups on the surface of PVA contribute to its good surface wettability and enhance the mobility of the ions in the electrolyte solution. This indicates that a PVA sponge provides much faster access of ions to aqueous electrolytes, such as H_2SO_4, than do the melamine and PU sponges, due to its hydrophilic surface. In addition, the CV curves in Fig. 3e show that the RGO-PVA sponge can be operated over a wide range of scan rates, from 100 up to 1000 mV/s. This means fast ion diffusion inside the RGO-PVA sponge electrode, even at high scan rates.

Fig. 4a shows the galvanostatic charge-discharge curves of the RGO-PVA, RGO-melamine, and RGO-PU sponges at a constant current density of 5 A/g. All of the curves are quasi-triangular, which indicates the contribution of electric double-layer capacitance [20,26]. The specific capacitance values are calculated from galvanostatic charge-discharge curves according to the Eq. (1):

$$C_s = I\Delta t / m\Delta V \tag{1}$$

where C is the specific capacitance (F/g), I is the charge-discharge current, Δt is the time variation of the discharge, ΔV is the charge voltage range (1.0 V in the measurements in this paper), and m is the mass of the RGO in the RGO-sponge electrode. Fig. 4b shows that the highest specific capacitance values of the RGO-PVA, RGO-melamine, and RGO-PU sponges were 122.7, 101.0, and 55.56 F/g, respectively. The specific capacitance values of the RGO-PVA sponge, as expected, were higher than those of the other sponge types. After the current density was changed from 1 to 30 A/g, the capacitance retention ratios of the RGO-PVA, RGO-melamine, and RGO-PU sponges were 60.9%, 61.0%, and 78.0%, respectively, indicating the maintenance of stable capacitance values. To evaluate the cycle stability of the RGO-PVA sponge, a galvanostatic charge-discharge test was carried out at a current density of 5 A/g for 1000 cycles, as in Fig. 4c. The cycling stability test of the RGO-PVA sponge shows 87.4% capacitance retention after 1000 cycles. This good cycling stability demonstrates that the degradation of graphene
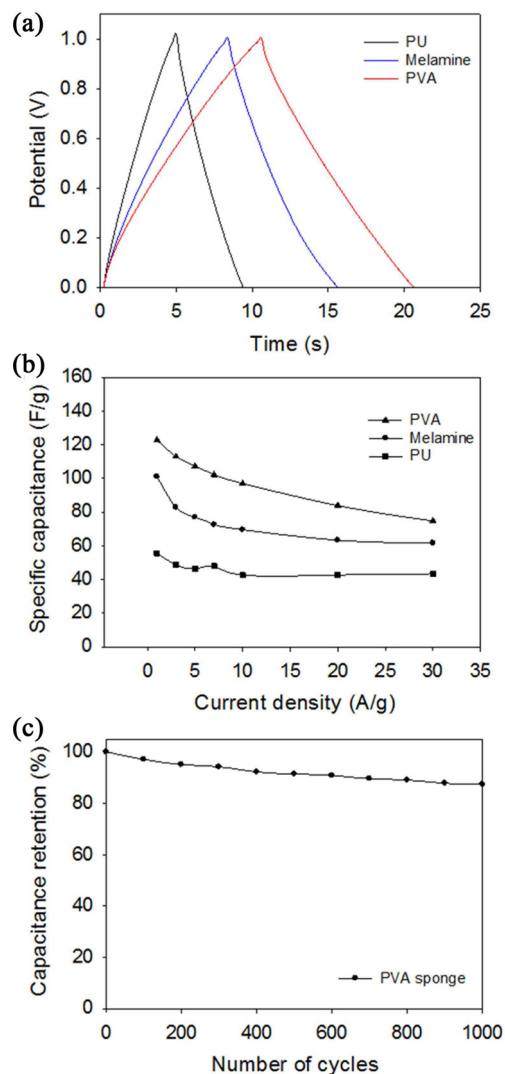

Fig. 4. (a) Galvanostatic charge-discharge curves of RGO coated PVA, melamine, and PU sponge at cyrrent density of 5 A/g. (b) The specific capacitance values. Of RGO-coated PVA, melamine, and PU sponge at different current densities from 1 to 30 A/g. (c) Cycling performance of RGO coated PVA sponge at a current density of 5 A/g
RGO, reduced graphene oxide; PVA, polyvinyl alcohol; PU, polyurethane.

has been alleviated as a result of the structural stability provided by using a sponge as the supporting substrate, and the fast diffusion of ions to the electrolyte then onto the surface of the coated graphene sheets in a PVA sponge.

A facile and reasonable dip and dry method was proposed for fabricating an RGO-sponge supercapacitor using several types of sponge as the supporting substrate. Among these, the PVA sponge with abundant hydroxyl groups provides the fastest access of ions to aqueous electrolytes, such as H_2SO_4. This is because of its extremely hydrophilic surface due to the hydroxyl groups. The synergetic combination of RGO and the PVA sponge has shown good capacitance performance through improved wettability, good ionic diffusion from electrolyte to electrode, and structural stability, which together have alleviated the degradation of graphene. The RGO-PVA sponge super-

capacitor demonstrated the highest specific capacitance value (122.7 F/g) at the current density of 1 A/g. This is an outstanding performance achieved by operating even at high scan rates of 1000 mV/s. Its good cycling stability was indicated by 87.4% capacitance retention after 1000 cycles. The RGO-PVA sponge supercapacitor provides a valuable and promising tool for energy storage devices.

Conflict of Interest

No potential conflict of interest relevant to this article was reported.

Acknowledgements

References

[1] Lin Z, Liu Y, Yao Y, Hildreth OJ, Li Z, Moon K, Wong CP. Superior capacitance of functionalized graphene. J Phys Chem C, **115**, 7120 (2011). http://dx.doi.org/10.1021/jp2007073.

[2] Zhao B, Liu P, Jiang Y, Pan D, Tao H, Song J, Fang T, Xu W. Supercapacitor performances of thermally reduced graphene oxide. J Power Sources, **198**, 423 (2012). http://dx.doi.org/10.1016/j.jpowsour.2011.09.074.

[3] Kötz R, Carlen M. Principles and applications of electrochemical capacitors. Electrochim Acta, **45**, 2483 (2000). http://dx.doi.org/10.1016/s0013-4686(00)00354-6.

[4] Chu A, Braatz P. Comparison of commercial supercapacitors and high-power lithium-ion batteries for power-assist applications in hybrid electric vehicles: I. initial characterization. J Power Sources, **112**, 236 (2002). http://dx.doi.org/10.1016/s0378-7753(02)00364-6.

[5] Burke A. Ultracapacitors: why, how, and where is the technology. J Power Sources, **91**, 37 (2000). http://dx.doi.org/10.1016/s0378-7753(00)00485-7.

[6] Halper MS, Ellenbogen JC. Supercapacitors: A Brief Overview, The MITRE Corporation, McLean, VA (2006).

[7] Conway BE. Transition from "Supercapacitor" to "Battery" Behavior in Electrochemical Energy Storage. J Electrochem Soc, **138**, 1539 (1991). http://dx.doi.org/10.1149/1.2085829.

[8] Conway BE, Birss V, Wojtowicz J. The role and utilization of pseudocapacitance for energy storage by supercapacitors. J Power Sources, **66**, 1 (1997). http://dx.doi.org/10.1016/s0378-7753(96)02474-3.

[9] Stoller MD, Park S, Zhu Y, An J, Ruoff RS. Graphene-based ultracapacitors. Nano Lett, **8**, 3498 (2008). http://dx.doi.org/10.1021/nl802558y.

[10] Pumera M. Electrochemistry of graphene: new horizons for sensing and energy storage. Chem Rec, **9**, 211 (2009). http://dx.doi.org/10.1002/tcr.200900008.

[11] Novoselov KS, Geim AK, Morozov SV, Jiang D, Zhang Y, Dubonos SV, Grigorieva IV, Firsov AA. Electric field effect in atomically thin carbon films. Science, **306**, 666 (2004). http://dx.doi.org/10.1126/science.1102896.

[12] Geim AK, Novoselov KS. The rise of graphene. Nat Mater, **6**, 183 (2007). http://dx.doi.org/10.1038/nmat1849.

[13] Lv W, Xia Z, Wu S, Tao Y, Jin FM, Li B, Du H, Zhu ZP, Yang QH, Kang F. Conductive graphene-based macroscopic membrane self-assembled at a liquid–air interface. J Mater Chem, **21**, 3359 (2011). http://dx.doi.org/10.1039/c0jm02852e.

[14] Park S, Ruoff RS. Chemical methods for the production of graphenes. Nat Nanotechnol, **4**, 217 (2009). http://dx.doi.org/10.1038/nnano.2009.58.

[15] Stankovich S, Dikin DA, Piner RD, Kohlhaas KA, Kleinhammes A, Jia Y, Wu Y, Nguyen ST, Ruoff RS. Synthesis of graphene-based nanosheets via chemical reduction of exfoliated graphite oxide. Carbon, **45**, 1558 (2007). http://dx.doi.org/10.1016/j.carbon.2007.02.034.

[16] Moon IK, Lee J, Ruoff RS, Lee H. Reduced graphene oxide by chemical graphitization. Nat Commun, **1**, 73 (2010). http://dx.doi.org/10.1038/ncomms1067.

[17] Ge J, Yao HB, Hu W, Yu XF, Yan YX, Mao LB, Li HH, Li SS, Yu SH. Facile dip coating processed graphene/MnO_2 nanostructured sponges as high performance supercapacitor electrodes. Nano Energy, **2**, 505 (2013). http://dx.doi.org/10.1016/j.nanoen.2012.12.002.

[18] Chen W, Rakhi RB, Hu L, Xie X, Cui Y, Alshareef HN. High-performance nanostructured supercapacitors on a sponge. Nano Lett, **11**, 5165 (2011). http://dx.doi.org/10.1021/nl2023433.

[19] Hu L, Chen W, Xie X, Liu N, Yang Y, Wu H, Yao Y, Pasta M, Alshareef HN, Cui Y. Symmetrical MnO_2–carbon nanotube–textile nanostructures for wearable pseudocapacitors with high mass loading. Acs Nano, **5**, 8904 (2011). http://dx.doi.org/10.1021/nn203085j.

[20] Wu Q, Xu Y, Yao Z, Liu A, Shi G. Supercapacitors based on flexible graphene/polyaniline nanofiber composite films. Acs Nano, **4**, 1963 (2010). http://dx.doi.org/10.1021/nn1000035.

[21] Paredes JI, Villar-Rodil S, Solís-Fernández P, Martínez-Alonso A, Tascón JMD. Atomic force and scanning tunneling microscopy imaging of graphene nanosheets derived from graphite oxide. Langmuir, **25**, 5957 (2009). http://dx.doi.org/10.1021/la804216z.

[22] Fan X, Peng W, Li Y, Li X, Wang S, Zhang G, Zhang F. Deoxygenation of exfoliated graphite oxide under alkaline conditions: a green route to graphene preparation. Adv Mater, **20**, 4490 (2008). http://dx.doi.org/10.1002/adma.200801306.

[23] Zhou M, Wang Y, Zhai Y, Zhai J, Ren W, Wang F, Dong S. Controlled synthesis of large-area and patterned electrochemically reduced graphene oxide films. Chem Eur J, **15**, 6116 (2009). http://dx.doi.org/10.1002/chem.200900596.

[24] Meng Y, Wang K, Zhang Y, Wei Z. Hierarchical porous graphene/polyaniline composite film with superior rate performance for flexible supercapacitors. Adv Mater, **25**, 6985 (2013). http://dx.doi.org/10.1002/adma.201303529.

[25] Wang H, Hao Q, Yang X, Lu L, Wang X. A nanostructured graphene/polyaniline hybrid material for supercapacitors. Nanoscale, **2**, 2164 (2010). http://dx.doi.org/10.1039/c0nr00224k.

[26] Kim M, Lee C, Jang J. Fabrication of highly flexible, scalable, and high-performance supercapacitors using polyaniline/reduced graphene oxide film with enhanced electrical conductivity and crystallinity. Adv Funct Mater, **24**, 2489 (2014). http://dx.doi.org/10.1002/adfm.201303282.